THE JOURNAL OF PHYSICAL CHEMISTRY Letters

Letter

pubs.acs.org/JPCL

Methane Adsorption on Graphitic Nanostructures: Every Molecule Counts

Samuel Zöttl,[†] Alexander Kaiser,[†] Peter Bartl,[†] Christian Leidlmair,[†] Andreas Mauracher,[†] Michael Probst,[†] Stephan Denifl,[†] Olof Echt,*[,†,‡] and Paul Scheier*[,†]

[†]Institut für Ionenphysik und Angewandte Physik, Universität Innsbruck, Techniker Strasse 25, A-6020 Innsbruck, Austria

[‡]Department of Physics, University of New Hampshire, Durham, New Hampshire 03824, United States

ABSTRACT: Bundles of single-walled nanotubes are promising candidates for storage of hydrogen, methane, and other hydrogen-rich molecules, but experiments are hindered by nonuniformity of the tubes. We overcome the problem by investigating methane adsorption on aggregates of fullerenes containing up to six C_{60}; the systems feature adsorption sites similar to those of nanotube bundles. Four different types of adsorption sites are distinguished, namely, registered sites above the carbon hexagons and pentagons, groove sites between adjacent fullerenes, dimple sites between three adjacent fullerenes, and exterior sites. The nature and adsorption energies of the sites in C_{60} aggregates are determined by density functional theory and molecular dynamics (MD) simulations. Excellent agreement between experiment and theory is obtained for the adsorption capacity in these sites.

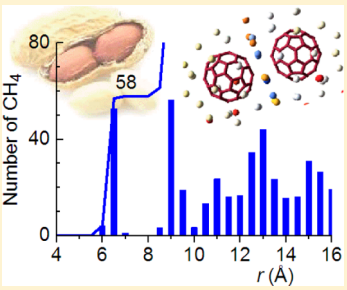

SECTION: Surfaces, Interfaces, Porous Materials, and Catalysis

Adsorption of hydrogen, methane, and other hydrocarbons in porous carbonaceous materials shows promise for high-density storage of hydrogen-rich molecules.[1−9] Methane is of interest because of its dominance in natural gas and potential use in fuel cells; graphite, graphene, and bundles of nanotubes have been considered for its storage.[10,11] Gases adsorbed on graphitic nanostructures are also of interest in basic science because the systems exhibit fascinating phenomena that depend on the dimensionality and corrugation of the surface.[3,12] Weak corrugation arises from the atomistic structure of graphite or graphene; over curved convex surfaces, the adsorption energy decreases, whereas the strength of the corrugation increases.[13,14] Bundles of nanotubes[14−19] and layers of fullerenes[20,21] offer additional, stronger adsorption sites. However, experiments involving nanotubes are hampered by their heterogeneity, the presence of impurities including metal catalysts used for tube synthesis, and the presence of uncapped tubes; these factors make it difficult to determine the nature, storage capacities, and energies of adsorption sites.[2,16−19]

Some of these difficulties may be avoided in experiments on individual nanotubes,[22] but questions remain about the exact nature of those tubes,[23] and they do not offer sites characteristic of bundles. In the present work, we solve the problem by studying small C_{60} aggregates, which represent, in a way, the ultimate bundle of capped, single-walled nanotubes; they are strictly uniform, with the smallest possible values for length (zero) and diameter (10 Å). They offer the same types of adsorption sites as bundles of nanotubes, namely, groove sites between adjacent tubes, and registered exterior sites.[14−16,19,24] For C_{60} trimers and beyond, they also offer dimple sites that are characteristic of close-packed layers of C_{60}.[20] We determine the adsorption capacity in the various sites by direct weighing, that is, by mass spectrometry.

CH_4 is adsorbed on C_{60} aggregates by passing cold, superfluid helium nanodroplets through cells that contain C_{60} and CH_4 vapor at suitably chosen pressures.[25,26] A section of a mass spectrum of $C_{60}(CH_4)_n$ is displayed in Figure 1a. For each value of n, a group of peaks spaced by 1 u is observed. Two factors cause these multiplets, (i) contributions from ions that contain one or more ^{13}C isotopes (natural abundance 1.07%) and (ii) contributions from "nonstoichiometric" ions that result from ion−molecule reactions after ionization.[27,28] $[C_{60}(CH_4)_{n-1}CH_5]^+$ is the most abundant of these; others have the composition $[C_{60}(CH_4)_{n-2}C_2H_x]^+$, with $x \leq 7$. Our focus is on the dominant series, stoichiometric $[C_{60}(CH_4)_n]^+$.

The abundance of $[C_{60}(CH_4)_n]^+$ (Figure 1a) features a prominent local maximum at $n = 32$, which coincides with the number of pentagonal (12) and hexagonal (20) faces of C_{60}. Thus, in agreement with recent studies of $[C_{60}He_n]^+$ and $[C_{60}(H_2)_n]^+$,[29,30] adsorption of one molecule per fullerene facet produces ions of enhanced stability (the correlation between ion abundance and energetic stability has been discussed elsewhere[31]).

The size dependence of the abundance of methane adsorbed on aggregates of C_{60}, $[(C_{60})_m(CH_4)_n]^+$ exhibits anomalies in the mass regions displayed in Figure 1b−e. Abrupt, statistically significant drops occur at $[(C_{60})_2(CH_4)_7]^+$, $[(C_{60})_3(CH_4)_{13}]^+$, $[(C_{60})_4(CH_4)_{16}]^+$, and $[(C_{60})_5(CH_4)_{21}]^+$.

The abundance of $[(C_{60})_m(CH_4)_n]^+$ extracted from mass spectra is summarized in Figure 2a. The C_{60} aggregates feature one or two clearly discernible anomalies up to the C_{60} pentamer; anomalies are particularly strong for the tetramer.

Received: August 3, 2012
Accepted: August 28, 2012
Published: August 28, 2012

   dx.doi.org/10.1021/jz301106x | J. Phys. Chem. Lett. 2012, 3, 2598−2603

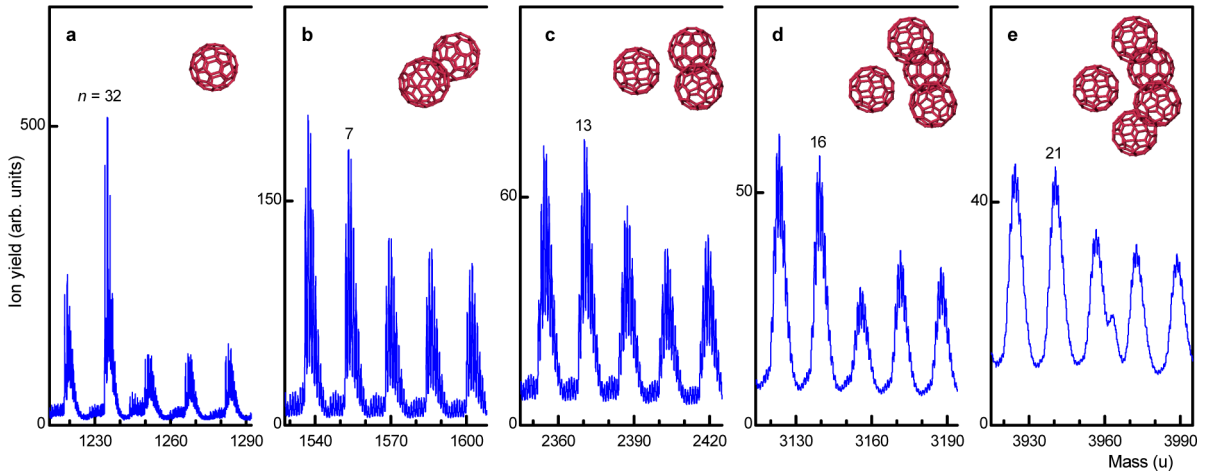

Figure 1. Mass spectra of helium droplets doped with C_{60} and CH_4. The most prominent ions have the stoichiometry $[(C_{60})_m(CH_4)_n]^+$, with m = 1−5 (a−e). The sections shown reveal the most significant abundance anomalies for each series.

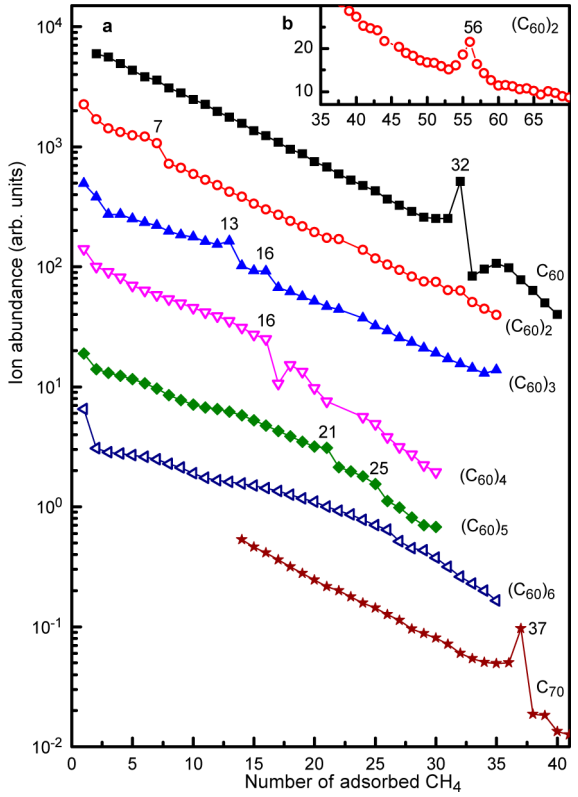

Figure 2. Ion abundance of C_{60}−CH_4 complexes deduced from mass spectra. The main panel displays data for $[(C_{60})_m(CH_4)_n]^+$ versus n on a logarithmic scale for complexes containing up to six C_{60}; also shown is the abundance of $[C_{70}(CH_4)_n]^+$. Statistically significant anomalies are labeled with the value of n. The abundance of $[(C_{60})_2(CH_4)_n]^+$ at around n = 56 is displayed in the inset.

The analysis of complexes containing more than 44 CH_4 units is problematic because $(CH_4)_{45}$ has the same nominal mass as C_{60}. Nevertheless, motivated by calculations discussed below, we have been able to determine the abundance of $[(C_{60})_2(CH_4)_n]^+$ up to n = 70 by optimizing the partial pressures of C_{60} and CH_4 in the cells where helium nanodroplets are doped. A local maximum is observed at n = 56 (see the inset in Figure 2).

Also shown in Figure 2a are data for $[C_{70}(CH_4)_n]^+$; they feature an anomaly at n = 37, very similar in shape to that at $[C_{60}(CH_4)_{32}]^+$. In fact, the interpretation is the same: the system attains high stability when each of the 37 faces of C_{70}^+ (which has 12 pentagons + 25 hexagons) is decorated by one CH_4.

Insight into the origin of the anomalies in the ion abundance is gained from molecular dynamics (MD) simulations for charged C_{60} aggregates complexed with CH_4. The CH_4 adsorption energy is highest when one of the four faces of the CH_4 tetrahedron is parallel to a hexagon of C_{60}^+, with a binding energy of 117 meV. For the neutral complex, the value is 115 meV. One reason for this surprisingly small effect of the C_{60} net charge is the low partial charge (~0.02 e_0) per carbon atom, of which only approximately six are so close to CH_4 that the short-ranged polarization/induction makes a difference.

The corresponding values over pentagons are 115 and 108 meV, respectively, higher than the 96 meV computed by Akai et al. for CH_4 on graphene.[14] The bond strength of the CH_4−CH_4 dimer is an order of magnitude weaker (10.8 meV). Thus, the $[(C_{60})_m(CH_4)_n]^+$ system is dominated by the $[C_{60}$−$C_{60}]^+$ interaction (413 meV with the PBE1PBE functional without counterpoise) and the CH_4−substrate interaction.

Figure 3 shows representative snapshots of charged aggregates containing 2−4 C_{60} plus 80 CH_4. Color indicates the energy of adsorbed CH_4, computed as a sum over all pairwise interactions. Molecules in the "grooves" between any pair of adjacent fullerenes are strongly bound; these regions are most clearly seen, and marked, in the bottom of Figure 3a (dimer) and b (trimer). A subset of groove sites are those that are equidistant to three C_{60}; these "dimple" sites are located on the C_3 symmetry axes of the trimer and tetrahedral tetramer; in the projected view of the trimer, they appear at the center (bottom of Figure 3b).

A layer of more weakly bound molecules wraps around the C_{60} aggregate. For the dimer, this first layer resembles the shell of a peanut; its members appear white in Figure 1a or blue because groove sites are a subset of the first layer. In the following analysis, we will attempt to determine the exact number of molecules in these various adsorption sites and compare them with experiment.

Simulations were run for charged C_{60} aggregates with 50, 80, or 500 CH_4 attached. Calculations with more than 500

dx.doi.org/10.1021/jz301106x | J. Phys. Chem. Lett. 2012, 3, 2598−2603

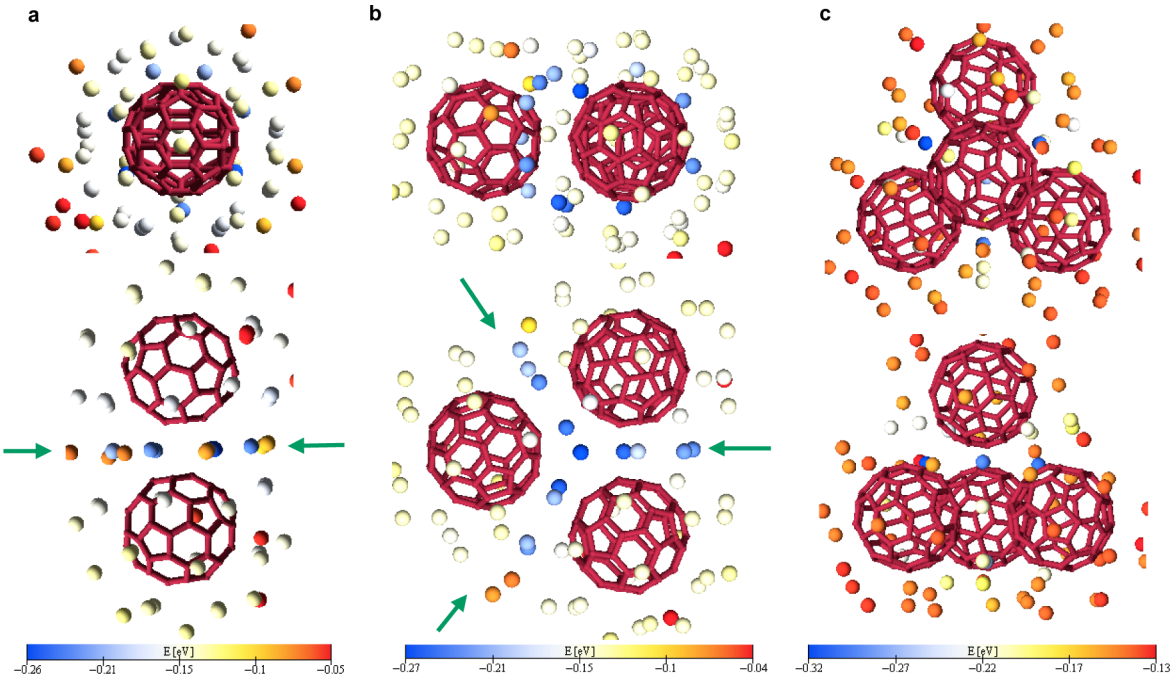

Figure 3. Energy-resolved snapshots of C_{60} dimer, trimer, and tetramer ions (a−c) with 80 adsorbed CH_4. Each complex is viewed from two different perspectives. CH_4 molecules are represented as spheres even though the energy dependence of their orientation is included in the calculations. The color of the molecules represents their energy, computed as a sum over all pairwise interactions with the fullerenes and all other CH_4. Strongly bound methanes (blue) reside in the "grooves", which are marked by arrows for the dimer and trimer.

molecules were too time-consuming; calculations with 50 or 80 molecules revealed some features more clearly. Molecular coordinates and energies were registered every 2 ps over a simulation time of 400 ps. From these data, we extracted the time-averaged spatial and energy distributions of the adsorbate; they are presented in Figure 4 as histograms for the fullerene monomer through tetramer. The upper-left histogram in each group shows the spatial distribution of CH_4 versus the distance from the center of the nearest fullerene (r_{min}). For the monomer, this is simply the radial distribution; the first layer is comprised of 32 molecules and has a very narrow distribution that peaks at $r \approx 6.75$ Å. Additional molecules are located at much larger distances. In other words, the commensurate layer with one CH_4 per fullerene facet completes the first monolayer. The situation contrasts with the results observed for He, where the commensurate layer with 32 He leaves room for 28 additional He at nearly the same distance from the C_{60} center.[29] The size of CH_4 happens to be just right to make the commensurate layer coincide with the first complete monolayer; the effect of this shell closing on the binding energy and ion abundance is consequently large.

The C_{60} dimer ion (Figure 4b) features a similarly distinct first layer with 58 molecules (the computed value depends slightly on the total number of adsorbed CH_4; the simulations shown here involved 500 CH_4). The value is in good agreement with the experimental value, $n = 56$ (Figure 2b). The calculations predict similarly distinct adsorbate layers of ∼80 molecules for $(C_{60})_3^+$ (see the upper-left histogram in Figure 4c) and ∼100 for $(C_{60})_4^+$ (Figure 4d), which are beyond the reach of experiments.

In order to reveal the number of adsorbate molecules that reside in groove sites, we present histograms in Figure 4 that count molecules within a thin layer located midway between pairs of adjacent C_{60}. A molecule is considered to be in a groove site if the distances to the two nearest C_{60} are equal within a tolerance $\varepsilon = 1$ Å. The histograms reveal that 7, 13, and 17 molecules reside in groove sites of the dimer, trimer, and tetramer, respectively; the values agree nicely with the observed anomalies at 7, 13, and 16 in the abundance of the corresponding ions.

The calculated values do not change if n and the tolerance ε are varied within reasonable bounds. For example, we have obtained the same number of groove sites for $n = 80$; for even larger values of n, one observes the onset of a second layer in the groove region. Features become blurred if large numbers (500) of CH_4 are adsorbed; they exert additional forces on the innermost layer. In a future publication, we will explore the effects of n and ε in more detail.

Another way to reveal the adsorption capacity of specific sites is by looking at the energies of adsorbate molecules. After all, it is the adsorption energy that will directly affect the experimental abundance distributions.[29,31] The corresponding energy histograms in Figure 4 confirm our conclusions drawn so far; 32 molecules are particularly strongly bound to C_{60}^+. For the dimer, the seven CH_4 in groove sites are most strongly bound. In MD simulations of $[(C_{60})_2(CH_4)_{500}]^+$ (not shown), this feature becomes blurred, but instead, the completion of an adsorbate layer at $n \approx 58$ appears. Thirteen CH_4 in groove sites are energetically favored for the C_{60} trimer (Figure 4c). There is a hint of substructure, with two very strongly bound molecules in the two dimple sites of the C_{60} trimer. The energy histogram of the tetramer (Figure 4d) shows a distinct substructure, namely, 4 molecules in the dimples of the tetrahedral C_{60} tetramer plus 13 additional molecules in groove sites.

This substructure can, indeed, be identified in the experimental ion abundance if the data are divided by a smooth function, a standard procedure in cluster science.[32,33] We chose a third-order polynomial that was fit to nine data

dx.doi.org/10.1021/jz301106x | J. Phys. Chem. Lett. 2012, 3, 2598−2603

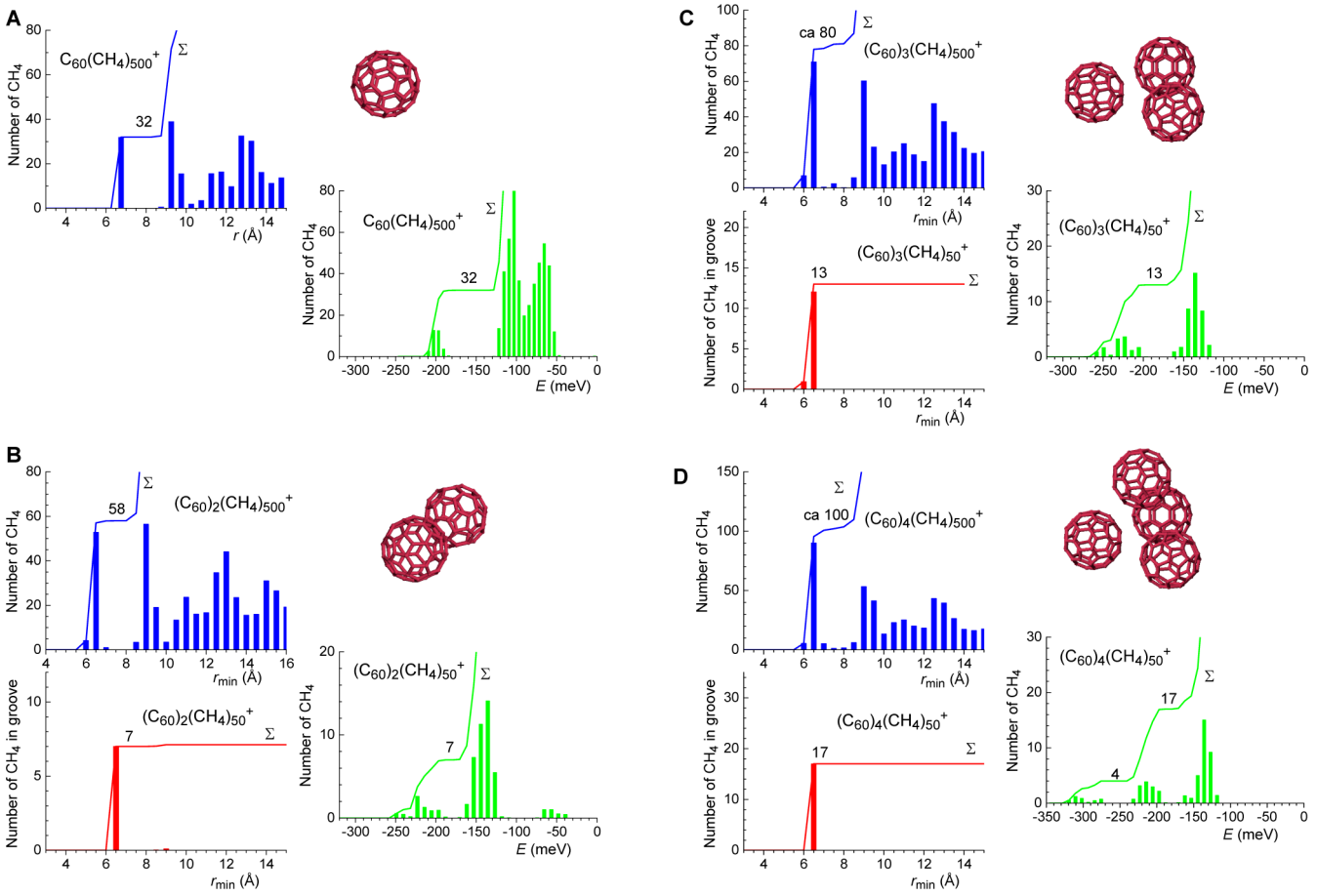

Figure 4. Structures and energetics extracted from MD simulations. For each panel, the histogram to the upper left (blue) represents the number of adsorbed CH_4 in $[(C_{60})_m(CH_4)_{500}]^+$ versus the distance from the center of the nearest fullerene; solid lines represent the accumulated sum $\sum$ of molecules. These histograms reveal the number of molecules in complete adsorbate layers. The histograms below (in red) reveal the number of molecules that are located in groove or dimple sites. The energy histograms (green) show the number of adsorbed molecules versus their energy.

points. Details of the procedure have been discussed previously;[31] results are shown in Figure 5. Anomalies appear at n = 2 for the trimer and 4 for the tetramer, in excellent agreement with theory (and straightforward geometric reasoning).

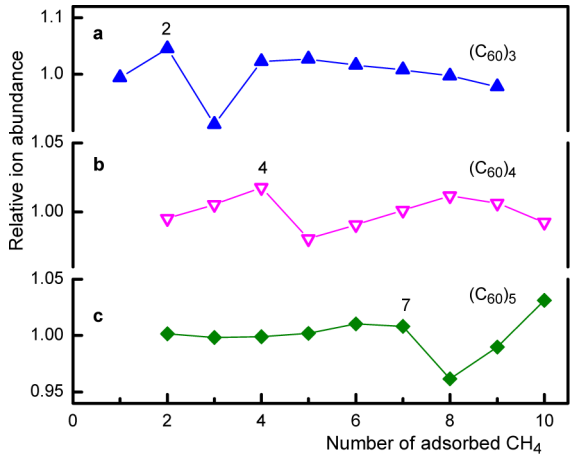

Figure 5. The experimental ion abundance divided by a smooth function reveals another, rather weak anomaly. For the C_{60} trimer and tetramer, the numbers (2 and 4, respectively) agree with the number of dimple sites.

The anomaly observed at n = 7 for the pentamer is not yet understood though. Calculations with a variety of realistic interaction potentials predict that the energetically preferred structure of $(C_{60})_5$ is the trigonal bipyramid[34,35] which has six trigonal faces, that is, six dimple sites. The positive charge could possibly change the structure, but the square pyramid that is the second best structure for neutral systems provides no rational either; it would have five dimple sites, four at the centers of the trigonal faces and one at the square.

In conclusion, we have identified four different sites for adsorption of CH_4 on charged, isolated aggregates of C_{60}. The nature and energies of the sites are revealed by MD simulations; they correspond to sites over the hexagonal or pentagonal facets of C_{60}, groove sites for the dimer and beyond, dimples sites for the trimer and beyond, and the first complete adsorption layer for the dimer. Excellent agreement between experiment and theory is obtained for the storage capacity of the sites.

METHODS

Experimental Section. Aggregates of C_{60} or C_{70} were synthesized and subsequently exposed to methane inside of superfluid helium nanodroplets. The nanodroplets were produced by expanding helium from a stagnation pressure of approximately 2 MPa through a 5 μm nozzle, cooled to about 8 K, into vacuum. The average number of helium atoms per droplet

dx.doi.org/10.1021/jz301106x | J. Phys. Chem. Lett. 2012, 3, 2598−2603

formed in the expansion was on the order of 5×10^5; the droplets cool to a temperature of ~0.37 K by evaporation.[25,36] The skimmed supersonic beam of helium droplets traversed two pickup cells. The first cell was filled with low-pressure C_{60} or C_{70} (SES Corp., purity 99.95%), which was vaporized from a crucible; methane at partial pressures ranging from 1×10^{-3} to 4×10^{-3} Pa was present in the second cell. Fullerene−methane complexes grew in the helium droplets upon successive collisions with the dopant molecules.[25,26] In some experiments, the droplets were doped with CH_4 before being doped with C_{60}; in another set of experiments, only one pickup region filled with C_{60} and CH_4 was used. The different procedures resulted, by and large, in similar mass spectra. After the pickup region, the doped helium droplets passed a region in which they were ionized by electron impact at 70 eV. Cations were accelerated into the extraction region of a commercial time-of-flight mass spectrometer equipped with a reflectron; its mass resolution was about $\Delta m/m = 1/5000$. Additional experimental details have been described elsewhere.[37,38]

Theory. We used classical MD simulations in combination with force fields constructed from quantum mechanical calculations. In the MD simulations, C_{60} and CH_4 were considered rigid. The fullerene aggregate was space-fixed at its optimized geometry; one of the fullerenes carried the charge. The intermolecular forces were represented by analytical atom−atom pair potentials. For the fullerene−methane force field, density functional calculations with the long-range and dispersion-corrected density functional ωB97X-D[39] in combination with Pople's[40] 6-31g(d,p) basis set (976 points) were performed. Methane was, as expected, slightly deeper bound to C_{60}^+ than to neutral C_{60}; otherwise, the potentials were very similar. The database for the methane−methane force field was derived from coupled cluster CCSD[41] calculations with Dunning's[42] correlation-consistent triple-ζ (cc-pVTZ) basis set (816 points).The analytical force fields were retrieved by a nonlinear fitting procedure. The DL_POLY_4 simulation package[43] was used for the MD simulations (simulation parameters: $T = 4$ K, $\Delta t = 2$ fs, overall simulation time 400 ps), while for the quantum chemical calculations, the Gaussian 09 A.02 program suite[44] was used.

AUTHOR INFORMATION

Corresponding Author

*E-mail: olof.echt@unh.edu (O.E.); paul.scheier@uibk.ac.at (P.S.).

Notes

The authors declare no competing financial interest.

ACKNOWLEDGMENTS

C.L. and P.B. acknowledge a dissertation grant from the vice-rectorate for research of the University of Innsbruck. This work was supported by the Austrian Science Fund, Wien (FWF, Projects P19073, L633, and J2973-N20). Part of this work was supported by the Austrian Ministry of Science BMWF as part of the UniInfrastrukturprogramm of the Research Platform Scientific Computing at the University of Innsbruck and was funded by the Austrian Science Fund (FWF) DK+ project Computational Interdisciplinary Modeling, W1227.

REFERENCES

(1) Crabtree, G. W.; Dresselhaus, M. S. The Hydrogen Fuel Alternative. *MRS Bull.* **2008**, *33*, 421−428.

(2) Arai, M.; Utsumi, S.; Kanamaru, M.; Urita, K.; Fujimori, T.; Yoshizawa, N.; Noguchi, D.; Nishiyama, K.; Hattori, Y.; Okino, F.; et al. Enhanced Hydrogen Adsorptivity of Single-Wall Carbon Nanotube Bundles by One-Step C_{60}-Pillaring Method. *Nano Lett.* **2009**, *9*, 3694−3698.

(3) Terrones, M.; Botello-Méndez, A. R.; Campos-Delgado, J.; López-Urías, F.; Vega-Cantú, Y. I.; Rodríguez-Macías, F. J.; Elías, A. L.; Muñoz-Sandoval, E.; Cano-Márquez, A. G.; Charlier, J.-C.; et al. Graphene and Graphite Nanoribbons: Morphology, Properties, Synthesis, Defects and Applications. *Nano Today* **2010**, *5*, 351−372.

(4) Tylianakis, E.; Psofogiannakis, G. M.; Froudakis, G. E. Li-Doped Pillared Graphene Oxide: A Graphene-Based Nanostructured Material for Hydrogen Storage. *J. Phys. Chem. Lett.* **2010**, *1*, 2459−2464.

(5) Klontzas, E.; Tylianakis, E.; Froudakis, G. E. On the Enhancement of Molecular Hydrogen Interactions in Nanoporous Solids for Improved Hydrogen Storage. *J. Phys. Chem. Lett.* **2011**, *2*, 1824−1830.

(6) Liu, C. J.; Burghaus, U.; Besenbacher, F.; Wang, Z. L. Preparation and Characterization of Nanomaterials for Sustainable Energy Production. *ACS Nano* **2010**, *4*, 5517−5526.

(7) Jena, P. Materials for Hydrogen Storage: Past, Present, and Future. *J. Phys. Chem. Lett.* **2011**, *2*, 206−211.

(8) Wang, Q.; Jena, P. Density Functional Theory Study of the Interaction of Hydrogen with Li_6C_{60}. *J. Phys. Chem. Lett.* **2012**, *3*, 1084−1088.

(9) Teprovich, J. A.; Wellons, M. S.; Lascola, R.; Hwang, S. J.; Ward, P. A.; Compton, R. N.; Zidan, R. Synthesis and Characterization of a Lithium-Doped Fullerane ($Li_xC_{60}H_y$) for Reversible Hydrogen Storage. *Nano Lett.* **2012**, *12*, 582−589.

(10) Schlapbach, L.; Züttel, A. Hydrogen-Storage Materials for Mobile Applications. *Nature* **2001**, *414*, 353−358.

(11) Li, Y. M.; Somorjai, G. A. Nanoscale Advances in Catalysis and Energy Applications. *Nano Lett.* **2010**, *10*, 2289−2295.

(12) Gordillo, M. C.; Boronat, J. Phase Transitions of H_2 Adsorbed on the Surface of Single Carbon Nanotubes. *Phys. Rev. B* **2011**, *84*.

(13) Gordillo, M. C.; Boronat, J. ^{4}He on a Single Graphene Sheet. *Phys. Rev. Lett.* **2009**, *102*, 085303.

(14) Akai, Y.; Saito, S. First Principles Study of H_2 and CH_4 Physisorption on Carbon Nanotubes. *Jpn. J. Appl. Phys.* **2003**, *42*, 640−644.

(15) Kostov, M. K.; Calbi, M. M.; Cole, M. W. Phonons and Specific Heat of Neon and Methane on the Surface of a Nanotube Bundle. *Phys. Rev. B* **2003**, *68*, 245403.

(16) Bienfait, M.; Zeppenfeld, P.; Dupont-Pavlovsky, N.; Muris, M.; Johnson, M. R.; Wilson, T.; DePies, M.; Vilches, O. E. Thermodynamics and Structure of Hydrogen, Methane, Argon, Oxygen, and Carbon Dioxide Adsorbed on Single-Wall Carbon Nanotube Bundles. *Phys. Rev. B* **2004**, *70*, 035410.

(17) LaBrosse, M. R.; Shi, W.; Johnson, J. K. Adsorption of Gases in Carbon Nanotubes: Are Defect Interstitial Sites Important? *Langmuir* **2008**, *24*, 9430−9439.

(18) Nikitin, A.; Li, X. L.; Zhang, Z. Y.; Ogasawara, H.; Dai, H. J.; Nilsson, A. Hydrogen Storage in Carbon Nanotubes through the Formation of Stable C−H Bonds. *Nano Lett.* **2008**, *8*, 162−167.

(19) Albesa, A. G.; Fertitta, E. A.; Vicente, J. L. Comparative Study of Methane Adsorption on Single-Walled Carbon Nanotubes. *Langmuir* **2010**, *26*, 786−795.

(20) Trasca, R. A.; Cole, M. W.; Coffey, T.; Krim, J. Gas Adsorption on a C_{60} Monolayer. *Phys. Rev. E* **2008**, *77*, 041603.

(21) Gatica, S. M.; Cole, M. W. New Physics of Gases Adsorbed on or near Fullerenes. *J. Low Temp. Phys.* **2011**, *162*, 573−582.

(22) Wang, Z. H.; Wei, J.; Morse, P.; Dash, J. G.; Vilches, O. E.; Cobden, D. H. Phase Transitions of Adsorbed Atoms on the Surface of a Carbon Nanotube. *Science* **2010**, *327*, 552−555.

(23) Kim, H.-Y.; Cole, M. W.; Mbaye, M.; Gatica, S. M. Phase Behavior of Ar and Kr Films on Carbon Nanotubes. *J. Phys. Chem. A* **2011**, *115*, 7249−7257.

(24) Lueking, A. D.; Cole, M. W. Commensurate Phases of Gases Adsorbed on Carbon Nanotubes. *Phys. Rev. B* **2007**, *75*, 195425.

(25) Toennies, J. P.; Vilesov, A. F. Superfluid Helium Droplets: A Uniquely Cold Nanomatrix for Molecules and Molecular Complexes. *Angew. Chem., Int. Ed.* **2004**, *43*, 2622−2648.
(26) Echt, O.; Märk, T. D.; Scheier, P. Molecules and Clusters Embedded in Helium Nanodroplets. In *Handbook of Nanophysics*; Sattler, K., Ed.; CRC Press: New York, 2010; Vol. *2* (Clusters and Fullerenes).
(27) Farnik, M.; Toennies, J. Ion−Molecule Reactions in ^{4}He Droplets: Flying Nano-Cryo-Reactors. *J. Chem. Phys.* **2005**, *122*, 014307.
(28) Leidlmair, C.; Bartl, P.; Schöbel, H.; Denifl, S.; Märk, T. D.; Yang, S.; Ellis, A. M.; Scheier, P. Ionization of Methane Clusters in Helium Nanodroplets. *ChemPhysChem* **2011**, *13*, 469−476.
(29) Leidlmair, C.; Wang, Y.; Bartl, P.; Schöbel, H.; Denifl, S.; Probst, M.; Alcamí, M.; Martín, F.; Zettergren, H.; Hansen, K.; et al. Structures, Energetics and Dynamics of Helium Adsorbed on Isolated Fullerene Ions. *Phys. Rev. Lett.* **2012**, *108*, 076101.
(30) Leidlmair, C.; Bartl, P.; Schöbel, H.; Denifl, S.; Probst, M.; Scheier, P.; Echt, O. On the Possible Presence of Weakly Bound Fullerene−H_2 Complexes in the Interstellar Medium. *Astrophys. J. Lett.* **2011**, *738*, L4.
(31) An der Lan, L.; Bartl, P.; Leidlmair, C.; Jochum, R.; Denifl, S.; Echt, O.; Scheier, P. Solvation of Na^+, K^+ and Their Dimers in Helium. *Chem.—Eur. J.* **2012**, *18*, 4411−4418.
(32) Martin, T. P. Shells of Atoms. *Phys. Rep.* **1996**, *273*, 199−241.
(33) Prasalovich, S.; Hansen, K.; Kjellberg, M.; Popok, V. N.; Campbell, E. E. B. Surface Entropy of Rare-Gas Clusters. *J. Chem. Phys.* **2005**, *123*, 084317.
(34) Luo, Y. H.; Zhao, J. J.; Qiu, S. T.; Wang, G. H. Genetic-Algorithm Prediction of the Magic-Number Structure of $(C_{60})_N$ Clusters with a First-Principles Interaction Potential. *Phys. Rev. B* **1999**, *59*, 14903−14906.
(35) Doye, J. P. K.; Wales, D. J.; Branz, W.; Calvo, F. Modeling the Structure of Clusters of C_{60} Molecules. *Phys. Rev. B* **2001**, *64*, 235409.
(36) Hartmann, M.; Miller, R. E.; Toennies, J. P.; Vilesov, A. F. High-Resolution Molecular Spectroscopy of Van Der Waals Clusters in Liquid Helium Droplets. *Science* **1996**, *272*, 1631−1634.
(37) An der Lan, L.; Bartl, P.; Leidlmair, C.; Schöbel, H.; Jochum, R.; Denifl, S.; Märk, T. D.; Ellis, A. M.; Scheier, P. The Submersion of Sodium Clusters in Helium Nanodroplets: Identification of the Surface → Interior Transition. *J. Chem. Phys.* **2011**, *135*, 044309.
(38) Schöbel, H.; Bartl, P.; Leidlmair, C.; Denifl, S.; Echt, O.; Märk, T. D.; Scheier, P. High-Resolution Mass Spectrometric Study of Pure Helium Droplets, and Droplets Doped with Krypton. *Eur. Phys. J. D* **2011**, *63*, 209−214.
(39) Chai, J.-D.; Head-Gordon, M. Long-Range Corrected Hybrid Density Functionals with Damped Atom−Atom Dispersion Corrections. *Phys. Chem. Chem. Phys.* **2008**, *10*, 6615−6620.
(40) Hehre, W. J.; Ditchfield, R.; Pople, J. A. Self-Consistent Molecular Orbital Methods. 12. Further Extensions of Gaussian-Type Basis Sets for Use in Molecular Orbital Studies of Organic Molecules. *J. Chem. Phys.* **1972**, *56*, 2257−2261.
(41) Scuseria, G. E.; Janssen, C. L.; Schaefer, H. F., III. An Efficient Reformulation of the Closed-Shell Coupled Cluster Single and Double Excitation (CCSD) Equations. *J. Chem. Phys.* **1988**, *89*, 7382−7387.
(42) Dunning, T. H. Gaussian Basis Sets for Use in Correlated Molecular Calculations. I. The Atoms Boron through Neon and Hydrogen. *J. Chem. Phys.* **1989**, *90*, 1007−1023.
(43) Todorov, I. T.; Smith, W.; Trachenko, K.; Dove, M. T. DL_POLY_3: New Dimensions in Molecular Dynamics Simulations Via Massive Parallelism. *J. Mater. Chem.* **2006**, *16*, 1911−1918.
(44) Frisch, M. J.; Trucks, G. W.; Schlegel, H. B.; Scuseria, G. E.; Robb, M. A.; Cheeseman, J. R.; Scalmani, G.; Barone, V.; Mennucci, B.; Petersson, G. A. et al. *Gaussian 09*, revision A.1; Gaussian, Inc.: Wallingford, CT, 2009.